2025 IMEKO TC26 International Conference on
Metrology for Archaeology and Cultural Heritage
Bergamo, Italy, October 15-17, 2025

Multi-technical non-invasive analysis to prevent deterioration in varnish-coated oil-paintings

A. Dal Fovo[1*], L. Maestro-Guijarro[2], P.M. Carmona-Quiroga[3], R. Fontana[1], F. Rosi[4], M. Alunni Cardinali[5,4], A. Romani[5], L. Comez[6], C. Riminesi[7], M. Iwanicka[8], P. Targowski[9], M. Kowalska[9], A. Philippidis[10], P. Pouli[10], M. Castillejo[2], M. Oujja[2]

[1]*Istituto Nazionale di Ottica, CNR, Florence, Italy, *alice.dalfovo@ino.cnr.it*
[2]*Instituto de Química Física Blas Cabrera, CSIC, Madrid, Spain*
[3]*Instituto de Ciencias de la Construcción Eduardo Torroja, CSIC, Madrid, Spain*
[4]*Istituto di Scienze e Tecnologie Chimiche, CNR, Perugia, Italy*
[5]*Dipartimento di Chimica, Biologia e Biotecnologie, Università di Perugia, Perugia, Italy*
[6]*Istituto Officina dei Materiali, CNR, Perugia, Italy*
[7]*Istituto di Scienza del Patrimonio Culturale, CNR, Sesto Fiorentino, Italy*
[8]*Faculty of Fine Arts, Nicolaus Copernicus University in Toruń, Poland*
[9]*Institute of Physics, Faculty of Physics, Astronomy and Informatics, Nicolaus Copernicus University in Toruń, Poland*
[10]*Institute of Electronic Structure and Laser, FORTH, Heraklion, Crete, Greece*

***Abstract* – Detecting early signs of varnish degradation is essential to prevent damage to underlying paintings. Despite extensive research, the mechanisms behind varnish alteration remain not fully understood, especially regarding the influence of pigments and binders in the paint layer. This study evaluated the effects of thermo-hygrometric and photochemical ageing on dammar and acrylic resins, both as standalone layers and as coatings on titanium white and yellow ochre oil-paints. A range of non-invasive techniques was used to assess the optical, mechanical, and morphological changes in the varnish and paint layers. The results revealed that varnish composition, ageing conditions, and underlying paint materials all significantly impact varnish degradation. The outcomes of this multi-analytical monitoring, which integrates point-based and imaging data, can profitably contribute to the creation of a digital replica for paintings – i.e. a digital twin – and support the training of automated systems to detect and identify early-stage degradation.**

I. INTRODUCTION

Varnishes play a crucial role in the finishing process of oil paintings, serving both aesthetic and protective functions. They contribute to the optical uniformity of the paint surface by reducing light scattering, thereby enhancing gloss and color saturation [1]. The final appearance of an oil painting depends not only on the varnish's thickness and properties (such as molecular weight and, to a lesser extent, the refractive index), but also on the characteristics of the underlying paint layer (e.g., medium content, opacity), the optical interaction between the varnish and paint layer [2], and the ageing processes affecting both materials [3]. Despite extensive research, the complexity of concurrent degradation processes complicates a full understanding of these mechanisms, hindering effective preservation strategies. Photochemical reactions, giving rise to oxidized and polymerized products in the varnish's outermost layers, are the primary cause of the loss of mechanical properties. However, environmental factors such as humidity and temperature fluctuations also critically contribute to paint layer deterioration [4]. In historical varnished paintings, climate-induced cracking can lead to delamination and flaking [5], underscoring the need for preventive measures. To improve our understanding, it is essential to investigate how varnish degradation impacts the underlying painting and whether inorganic pigments affect varnish film deterioration. This requires monitoring optical changes, tracking the early stages of craquelure formation, detecting the development of crystalline structures within the paint, and identifying other key degradation markers.

This study evaluates the thermo-hygrometric and photochemical ageing effects ─ at both surface and subsurface levels ─ on natural (dammar resin) and synthetic (acrylic resin) varnishes, applied alone or over paint layers containing two common inorganic pigments: titanium dioxide and yellow ochre. A multi-scale, non-invasive analytical approach was employed, combining established techniques such as reflectance imaging

spectroscopy (RIS), colorimetry, laser scanning micro-profilometry (MP), and optical coherence tomography (OCT), with advanced methods such as non-linear optical microscopy in multiphoton excitation fluorescence modality (NLOM-MPEF) [6] and Brillouin Light Scattering (BLS) spectroscopy [7].

We developed a digitally-integrated multi-analytical protocol optimized for potential in situ application, which systematically correlates the optical, mechanical and morphological properties of varnish layers through advanced computational modeling. This approach enables high-resolution mapping of varnish degradation patterns, elucidating the complex interplay between compositional factors, environmental ageing conditions, and substrate-paint interactions. Furthermore, our methodology leverages hyperspectral imaging and automated surface metrology to generate multidimensional datasets, facilitating predictive analytics for early-stage degradation detection. These innovations establish a robust framework for data-driven preventive conservation, significantly enhancing the precision and scalability of deterioration diagnostics in painted artworks.

II. MATERIALS AND METHODS

1. *Samples and ageing procedures*

We prepared three identical sets of samples, #1, #2 and #3, each comprising six distinct material layer combinations. Each set was subjected to a different ageing protocol: photochemical ageing (Set #1), thermo-hygrometric ageing (Set #2), and natural drying (Set #3, serving as the reference).

The paint and/or varnish layers were applied to glass substrates. Two varnish types were used: natural dammar (Varnish Glossy 081, Talens) and synthetic acrylic (Acrylic Varnish Glossy 114, Talens), applied over oil-based paints containing either titanium dioxide (titanium white) or yellow ochre pigments. The paints (Talens-Rembrandt) were extended using a simple applicator to achieve a uniform thickness of approximately 100 µm.

The samples underwent artificially ageing to simulate the effects of indoor illumination (Set #1) and combined humidity-temperature stress (Set #2). Photochemical ageing was performed in a custom-built chamber, where the samples were irradiated using a filtered Xenon lamp ($\lambda > 330$ nm, spanning from UVA to the visible spectral range) under controlled ambient conditions (temperature T = 30°C, relative humidity RH = 35-45%). The average irradiance was maintained at 2×10^5 µW/ cm^2, a dosage approximating 400 years of museum light exposure [8].

2. *Colorimetry mapping with reflectance imaging spectroscopy (RIS)*

The multispectral scanner used in this study was developed at the National Institute of Optics (CNR-INO, Italy). The system employs a whiskbroom scanning approach combined with narrow-band filtering to simultaneously acquire 32 spectral bands (16 VIS + 16 NIR) and pointwise spectral data across the 395–2550 nm range. Colorimetric processing was performed using in-house Matlab® software, with the following parameters: CIELab76 colour space, CIE1931 standard observer, and the D65 illuminant. Colour differences (ΔE) were calculated as the Euclidean distance between the L*, a*, b* coordinates of corresponding pixels in RIS-derived images (before vs. after treatment).

3. *Spectral-Domain Optical Coherence Tomography (Sd-OCT)*

OCT cross-sectional analysis was performed with two different devices. The first system was a high-resolution portable Sd-OCT prototype. This instrument employs a broadband light source with a spectral range of 770–970 nm (peak intensity at 870 nm), achieving an axial resolution of 2.2 µm in varnish and a lateral resolution of 13 µm and a maximum field of view (FOV) 15 x 15 mm^2. The axial imaging range extends to 1.8 mm, with a probe power not exceeding 1.3 mW at the sample surface.

The second instrument was a Thorlabs Telesto-II OCT device, utilizing a superluminescent diode with a central wavelength of 1300 nm (bandwidth ~100 nm). This configuration provides an axial resolution of 5.5 µm in air. The optical system, featuring a lens with 36 mm effective focal length, (EFL), delivers a lateral resolution of 13 µm and a FOV of 10 × 10 mm^2, with a 3.5 mm imaging depth.

4. *Laser scanning micro-profilometry (MP)*

The micro-profilometer employed in this study is a custom-built system, integrating a conoscopic holography distance-meter (ConoProbe1000, Optimet) with a precision scanning system. The probe assembly consists of a 655 nm laser diode, a birefringent crystal positioned between two polarizers, and a CCD camera, mounted on high- precision motorized linear stages for XYZ displacements. For these measurements, the probe was equipped with a 50 mm lens, providing a 4 cm stand-off distance and 8 mm dynamic range, with 1 µm axial and 20 µm lateral resolution. To quantify artificial ageing effects, mean surface roughness was calculated over standardized 1 × 1.5 cm^2 areas (6×10^4 pixels) following a multi-stage filtering protocol, as shown in Fig. 1 for sample C from Set #3, as an example: median filtering for initial noise reduction and bad data removal; signal conditioning through planar alignment (Fig. 1a,b); low-frequency component removal by applying a Gaussian filter ($\sigma = 10$) to isolate surface roughness (Fig. 1b,c); elimination of brushstroke artifacts with a Gaussian filter ($\sigma = 2$), while preserving fine surface features (Fig. 1c,d). The application of appropriate filtering algorithms to separate high-frequency from lower-frequency components corresponds to macroscopic shape and surface waviness removal [9]. Roughness was quantified using the arithmetical mean height of the surface (Sa) and the root mean square roughness (Sq).

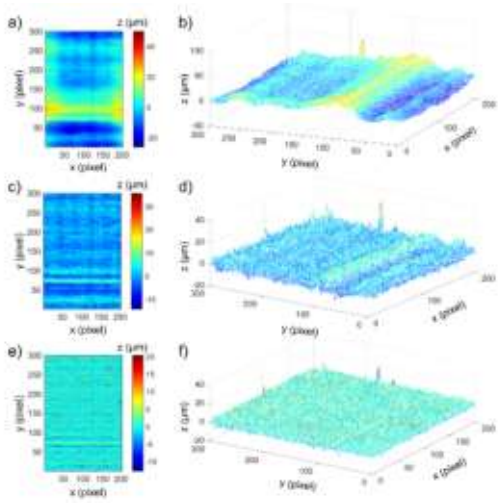

Fig. 1. MP data processing for roughness calculation on sample C from Set #3: 2D and 3D maps of the conditioned surface after best-fit plane subtraction (a,b), after low-frequency component filtering (c,d), and after high-frequency component filtering (e,f).

5. *Multiphoton excitation fluorescence (MPEF)*

The in-depth measurement of varnish degradation was performed using a homemade nonlinear optical microscope. The excitation source was a mode-locked Ti:Sapphire femtosecond (fs) laser (800 nm, 680 mW average power, 70 fs pulse width, 80 MHz repetition rate). Laser power was controlled with a variable neutral density filter (NDC-50C-2 M, Thorlabs). Varnish thickness quantification relied on MPEF signal-depth profiles, fitted with Lorentzian and/or top-hat functions (OriginPro 2018). The measured full-width half maximum (FWHM) values were corrected by the apparent depth correction factor F [6].

6. *Brillouin Light Scattering (BLS) spectroscopy*

BLS detects inelastic light scattering from thermally excited acoustic phonons, yielding insights into elastic properties such as sound velocity, density, and elastic moduli [10]. In this study, a single-mode 532 nm laser was focused on a 2 µm spot using a 20x objective (NA = 0.42). Backscattered light was analyzed with a high-resolution 3+3 tandem Fabry-Perot interferometer (6 mm mirror spacing). Laser power was kept below 2 mW to prevent photodamage. This configuration resolves Brillouin doublets arising from acoustic phonons, characterized by a frequency shift ω_0. The shift enables calculation of the material's sound velocity and longitudinal elastic modulus $M(\omega_0)$:

$$M(\omega_0) = \rho\, \lambda^2\, (\omega_0)^2 / 4n^2 \qquad (1)$$

where n and ρ are the refractive index and mass density of the sample, and λ is the laser wavelength. The frequency shift ω_0 is extracted by fitting the Brillouin spectrum to a damped harmonic oscillator (DHO) model:

$$I(\omega) = \frac{I_0}{\pi} \frac{\omega_0^2 \Gamma}{(\omega^2 - \omega_0^2)^2 + \omega^2 \Gamma^2} \qquad (2)$$

Here, I_0 is an amplitude factor dependent on the scattering cross- section, and Γ defines the width at half height of the Brillouin peak [7].

III. RESULTS

1. *Optical properties*

Colorimetric coordinates, namely L* (lightness), a* (red/green), and b* (yellow/blue), were analyzed as mean values across a standardized area of 1 × 1.5 cm² (2.400 pixels), as shown in Fig. 2 for single-layered dammar sample after natural (Fig. 2a) and photochemical (Fig. 2b) ageing. A total color difference (ΔE) map, presented as 2D color-coded plot (Fig. 2c), was derived from the corresponding ΔL*, Δa*, and Δb* maps (Fig. 2d-f).

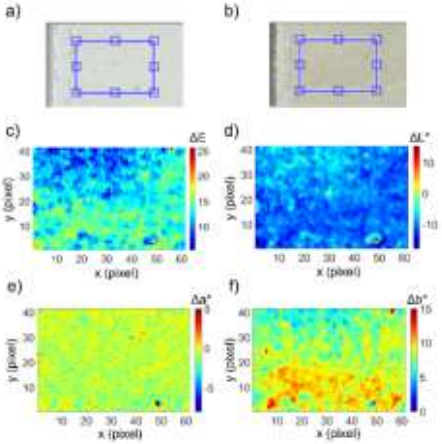

Fig. 2. Colour difference analysis for standalone dammar: visible light images of reference (a) and photo-aged sample (b), with the analysis area for mean value calculations (1 × 1.5 cm²) highlighted by a dotted rectangle); (c) colour-coded ΔE map of the selected area; (d-f) colour-coded distribution maps of ΔL, Δa*, and Δb* components, respectively.*

The most pronounced color changes occurred following photochemical ageing, particularly in samples containing dammar varnish (both alone and in combination with titanium dioxide or yellow ochre paints). In contrast, acrylic varnish exhibited significantly greater optical stability. Thermo-hygrometric ageing induced discernible alterations almost exclusively in dammar, particularly when applied over titanium white.

Acrylic varnish-based samples exhibited no measurable spectral modifications under either photochemical or thermo-hygrometric ageing, consistent with its optical stability observed in colorimetric analysis. This stark contrast with dammar underscores the synthetic varnish's resistance to environmental degradation.

2. *Varnish thickness and in-depth degradation*

The most significant variations in varnish thickness before and after ageing treatments occurred in dammar applied over titanium white: OCT thickness exhibited a substantial reduction (17–19 μm) after natural ageing contrasted by an expansion (10–12 μm) following thermo-hygrometric treatment. MPEF analysis reveals that photo-deterioration in dammar varnish predominantly affects surface layers, with diminishing impact at greater depths due to reduced oxidative penetration.

3. *Varnish surface morphology*

3D OCT showed significant alterations in dammar varnish surface morphology upon different ageing conditions (Fig. 3). Both as standalone layer (Fig. 3a,b) and applied over titanium white (Fig. 3c,d), dammar exhibited reduced surface homogeneity following thermo-hygrometric ageing (Fig. 3b,d), characterized by the development of discontinuities and irregular voids. Photochemical ageing exacerbated these effects, producing microcracks and bubble-like discontinuities (Fig. 3c) that may serve as initiation points for delamination or flaking. Similar degradation patterns emerged in dammar applied over yellow ochre (Fig. 3e,f), where photochemical ageing induced substantial cracking within the varnish layer (Fig. 3e).

These morphological changes in dammar correlate with the mechanical degradation of underlying paint substrates, which reflects their respective chemical stabilities.

In contrast, acrylic varnish maintained greater morphological stability, showing reduced surface homogeneity only after thermo-hygrometric ageing when applied over titanium white. This observation correlates with increased paint roughness in sample following thermo-hygrometric ageing. Notably, acrylic varnish over yellow ochre developed more extensive void formation after photochemical ageing, though to a lesser degree than observed in dammar systems.

4. *Paint roughness*

MP analysis revealed that photochemical ageing induced a significant increase in paint surface roughness in presence of dammar varnish, regardless of the pigment type, indicating that structural modifications in the varnish layer may propagate to the underlying paint. This effect is particularly pronounced in titanium dioxide paints. In contrast, thermo-hygrometric ageing caused more substantial roughness development in systems with acrylic varnish, especially those containing titanium white.

5. *Varnish visco-elastic properties*

BLS spectroscopy revealed distinct responses of varnishes to different ageing conditions. Photodegradation of dammar as both as single layer and in combination with TiO_2 (yellow lines in Fig. 4a, and b, respectively) produced a marked increase in stiffness relative to natural ageing (green lines), as evidenced by a shift of the BLS peak toward higher frequencies. Conversely, thermo-hygrometric ageing caused softening of the material, manifested by a BLS peak shift toward lower frequencies (blue lines). Notably, these mechanical responses remained consistent whether dammar was applied alone or in combination with TiO_2-oil paint, indicating minimal influence of this pigment on the varnish's ageing behavior.

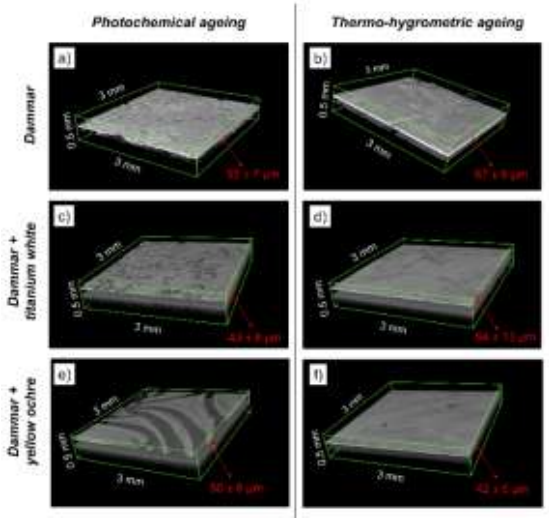

Fig. 3. Tomocubes of standalone dammar and combined with the paint layer, acquired using the 1300 nm OCT system, showing morphological alterations of the varnish surface following ageing treatments. The corrected mean varnish thickness (n = 1.5) is indicated in red.

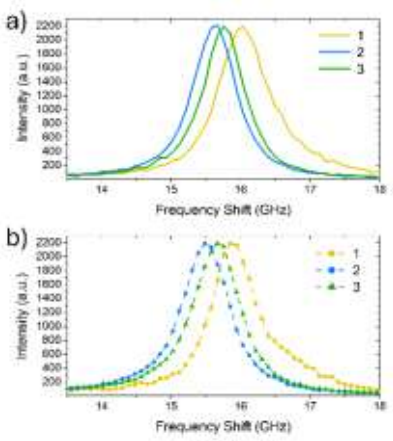

Fig. 4. BLS analysis of degradation effects in dammar varnish as a single layer (a) and laid over titanium white (b) subjected to photodegradation (#1, yellow line), thermo-hygrometric degradation (#2, blue line), and natural degradation (#3, green line).

Acrylic varnish demonstrated different mechanical characteristics under ageing conditions. While photodegradation similarly increased the material's rigidity, thermo-hygrometric ageing produced no

statistically significant alterations in its mechanical properties. A pronounced difference in absolute frequency values between dammar and acrylic varnishes was observed, reflecting their fundamentally distinct chemical compositions and microstructural organization.

IV. CONCLUSIONS

The multi-technique physical analysis of varnish/paint systems under various ageing conditions has revealed significant alterations in optical, morphological, structural, and mechanical properties of both varnish coatings and paint layers.

Photochemical ageing induces the most pronounced degradation effects, particularly in natural dammar varnish, which demonstrates greater susceptibility to color changes (yellowing, opacity, and brightness loss) compared to synthetic acrylic varnish.

Dammar varnish undergoes substantial photo-induced oxidation, fragmentation, and cross-linking reactions, primarily affecting surface layers and leading to increased rigidity. This results in craquelure formation, especially when applied over yellow ochre substrates. Similarly, acrylic varnish exhibits photo-induced stiffening but demonstrates superior overall stability against chemical and physical changes. NLOM-MPEF effectively characterized in-depth degradation patterns, revealing varnish-specific responses to different ageing conditions.

Natural ageing conditions cause significant thickness reduction in dammar varnish applied over titanium white, accompanied by increased surface roughness. Photochemical ageing additionally promotes chemical alterations in underlying paint layers, particularly affecting the oil binder in yellow ochre systems. While thermo-hygrometric ageing produces generally less severe effects, it induces measurable softening in dammar and reduces surface homogeneity in acrylic-titanium white systems.

These findings provide critical insights into the degradation mechanisms of artistic materials (varnishes and paints), offering scientific support for predictive conservation models, varnish selection criteria, and condition assessment protocols. The study establishes a robust framework for evaluating material stability that can directly inform conservation strategies for painted artworks. These results are suitable for implementing a digital twin dataset for paintings, contributing to the documentation of the current conservation state. A possible evolution of this approach is the introduction of smart sensors and AI-based data analysis to perform real-time monitoring, which will enable predictive maintenance and timely intervention.

Acknowledgements

The research was funded by H2020 European project IPERION HS (Integrated Platform for the European Research Infrastructure ON Heritage Science, GA 871034), PNRR H2IOSC (Humanities and Cultural Heritage Italian Open Science Cloud) Project (IR0000029) -CUP_B63C22000730005, funded by Next Generation EU. Funding from MCIN/AEI/10.13039/501100011033/FEDER, UE through the project PID2022-137017OB-I00 and from the Regional Government of Madrid through the project TEC Heritage-CM (TEC-2024/TEC-39) are acknowledged.

REFERENCES

[1] De la Rie, E. R. (1989). Old master paintings: a study of the varnish problem. Analytical chemistry, 61(21), 1228A-1240A.

[2] Berns, R. S., & De la Rie, E. R. (2003). The effect of the refractive index of a varnish on the appearance of oil paintings. Studies in conservation, 48(4), 251-262.

[3] Källbom, A., Nevin, A., & Izzo, F. C. (2021). Multianalytical Assessment of Armour Paints—The Ageing Characteristics of Historic Drying Oil Varnish Paints for Protection of Steel and Iron Surfaces in Sweden. Heritage, 4(3), 1141-1164.

[4] Bosco, E., Suiker, A. S., & Fleck, N. A. (2020). Crack channelling mechanisms in brittle coating systems under moisture or temperature gradients. International Journal of Fracture, 225, 1-30.

[5] Bosco, E., Suiker, A. S., & Fleck, N. A. (2021). Moisture-induced cracking in a flexural bilayer with application to historical paintings. Theoretical and Applied Fracture Mechanics, 112, 102779.

[6] Dal Fovo, A., Sanz, M., Mattana, S., Oujja, M., Marchetti, M., Pavone, F. S., ... & Castillejo, M. (2020). Safe limits for the application of nonlinear optical microscopies to cultural heritage: A new method for in-situ assessment. Microchemical Journal, 154, 104568.

[7] Alunni Cardinali, M., Cartechini, L., Paolantoni, M., Miliani, C., Fioretto, D., Pensabene Buemi, L., ... & Rosi, F. (2022). Microscale mechanochemical characterization of drying oil films by in situ correlative Brillouin and Raman spectroscopy. Science Advances, 8(26), eabo4221.

[8] Kokkinaki, O., Dimitroulaki, E., Melessanaki, K., Anglos, D., & Pouli, P. (2021). Laser-induced fluorescence as a non-invasive tool to monitor laser-assisted thinning of aged varnish layers on paintings: fundamental issues and critical thresholds. The European Physical Journal Plus, 136:938.

[9] He, B., Zheng, H., Ding, S., Yang, R., & Shi, Z. (2021). A review of digital filtering in evaluation of surface roughness. Metrology and Measurement Systems, 217-253.

[10] Bottani, C. E., & Fioretto, D. (2018). Brillouin scattering of phonons in complex materials. Advances in Physics: X, 3(1), 1467.